

# Thermally rounded depinning of an elastic interface on a washboard potential

A. B. Kolton and E. A. Jagla

*Centro Atómico Bariloche, Instituto Balseiro, Comisión Nacional de Energía Atómica, CNEA, CONICET, UNCUYO, Av. E. Bustillo 9500 R8402AGP S. C. de Bariloche, Río Negro, Argentina*

The thermal rounding of the depinning transition of an elastic interface sliding on a washboard potential is studied through analytic arguments and very accurate numerical simulations. We confirm the standard view that well below the depinning threshold the average velocity can be calculated considering thermally activated nucleation of forward moving defects. However, we find that the straightforward extension of this analysis to near or above the depinning threshold does not fully describe the physics of the thermally assisted motion. In particular, we find that exactly at the depinning point the average velocity does not follow a pure power-law of the temperature as naively expected by the analogy with standard phase transitions but presents subtle logarithmic corrections. We explain the physical mechanisms behind these corrections and argue that they are non-peculiar collective effects which may also apply to the case of interfaces sliding on uncorrelated disordered landscapes.

## I. INTRODUCTION

The depinning transition of elastic interfaces is a paradigmatic example of an out-of-equilibrium critical phenomenon. Its study is relevant for modeling diverse extended physical systems embedded in a quenched pinning potential. Often the pinning landscape acting in the interfaces is disordered such as in driven ferromagnetic [1] and ferroelectric [2, 3] domain walls, tension driven cracks [4–6], displacement of contact lines of liquid menisci [7–9] or earthquakes [10, 11]. In other cases the pinning landscape can be highly correlated or even periodic, such as the potential energy of the superconducting phase difference in long current driven Josephson junctions [12], or as in the case of field driven domain walls in artificial pinning potentials [13–15].

The basic phenomenology of depinning consists of an elastic manifold with an overdamped motion that interacts with a quenched potential energy landscape that tends to trap the interface in configurations in which the potential energy is minimized. When a uniform external driving force is applied, the interface remains pinned in a local minimum of the tilted energy potential if the amplitude of the driving force is below some well defined threshold, whereas otherwise it sets in a steady-state of motion with a well defined average velocity. The threshold value of the applied driving force defines the depinning force of the system  $f_c$ . When the driving force is slightly above the depinning threshold the velocity of the interface is expected to grow as a power law of the excess driving above the threshold value. This is just one indication that the kind of phenomenon occurring near  $f_c$  can be characterized as a (non-equilibrium) phase transition with critical properties [16–18].

The existence of a sharp depinning transition as a function of the driving force of an elastic interface depends crucially on the fact that thermal effects are negligible. If thermal fluctuations are important, then the depinning transition is smeared out, as for any finite applied force the interface can eventually jump forward via thermally

activated events over energy barriers, and hence the average velocity becomes different from zero for any non-zero driving force. It has been proposed that the effect of a small temperature on the depinning transition can be accounted for through an appropriate generalization of the scaling theory used at  $T = 0$ . In this respect, it has been suggested, either following a naive analogy with standard equilibrium phase transitions or by phenomenological nucleation theory arguments, that the effect of temperature on the depinning transition can be characterized by the value of a “thermal rounding” exponent  $\psi$ , that describes the average velocity  $v$  right at  $f_c$  as a function of temperature, namely  $v(f_c, T) \sim T^\psi$ . Regarding the velocity as the order parameter, the force as the control parameter and the temperature as a “symmetry-breaking field destroying the pinned phase” [19] such scaling proposal for the rounded depinning transition is analogous to the scaling with field  $H$  of the equilibrium Ising model magnetization  $M$  at the critical temperature  $T_c$ ,  $M(T_c) \sim H^{1/\delta}$  with  $\delta > 0$ , to cite the simplest example. The precise determination of the value of  $\psi$  has proven to be quite tricky however [20, 21], its universality questioned [22], and there is not yet a rigorous proof that the naive thermal rounding scaling theory is even consistent, in contrast with the zero temperature dynamics [18, 23–25] and the subthreshold creep dynamics [26–29].

In order to advance in the study of the thermal rounding of depinning-like transitions, we concentrate here in a case in which the zero-temperature limit provides an almost trivial result for the flux curve, and where the effect of temperature can be treated in a very accurate if not rigorous manner. This is the case of an elastic manifold evolving on a periodic pinning potential, the same for all individual sites of the elastic manifold, also known as a “washboard potential”. The model is on the other hand the celebrated overdamped Sine-Gordon dynamical model which has been used to model many different physical phenomena, such as overdamped coupled pendula, the equilibrium roughening transition [30], crystal-growth [31, 32], vortex matter in layered superconductors [33–36], forced soliton gases [37] and over-

damped long Josephson junctions driven by an external current [12]. It may be also used to model the dynamics of the internal degrees of freedom of an extended magnetic domain wall describing the axial rotation of the local magnetization vector, relevant for spintronics [38–40]. A proper understanding of the depinning transition of the Sine-Gordon model per se is hence also very important, as it is for instance related to the onset of rotation of torque driven coupled pendula, the onset of dissipation in superconducting systems such as Josephson junctions or vortex systems or to the Walker breakdown in magnetic domain wall systems.

In this paper we show, both through analytic arguments and very accurate numerical simulations, that the effect of temperature at the depinning transition in this simple extended model cannot be accounted for by a simple one-parameter scaling, and that it involves the appearance of subtle logarithmic corrections not precluded by any of the standard arguments made so far for the thermal rounding of the depinning transition. We thus expect that this qualitative behavior is not peculiar of the model, but applies for instance to the more standard and complicated case of uncorrelated disorder.

## II. MODEL

Consider an elastic interface (with short range interactions) in  $d$  spatial dimensions, characterized by its position  $h(r)$ . The interface feels the effect of an underlying periodic potential  $V(h)$ , and an external force  $f_0$ . The dynamical equations of the system are

$$\frac{\partial h(r, t)}{\partial t} = -\frac{dV(h)}{dh} + \nabla^2 h + f_0 + \sqrt{T}\eta(t, r) \quad (1)$$

where temperature has been introduced through the use of a standard Langevin formalism, with the white noise  $\eta$  characterized by

$$\langle \eta(t, r) \rangle = 0, \quad \langle \eta(t, r)\eta(t', r') \rangle = \delta(t - t')\delta^d(r - r') \quad (2)$$

At  $T = 0$  the dynamics of the system greatly simplifies, as the interface becomes flat [41], and its global position  $h$  follows the one-particle equation

$$\frac{\partial h}{\partial t} = -\cos(h) + f_0 \quad (3)$$

(from now on we specialize to a potential of the form  $V(h) = \sin(h)$ ). For  $f_0 < f_c = 1$  the interface does not move, whereas for  $f_0 > f_c$  there is a finite average velocity. For  $f_0$  slightly above  $f_c$ , the velocity  $v \equiv \langle \partial_t h \rangle$  scales as

$$v \sim \sqrt{f_0 - f_c} \quad (4)$$

which defines the flow exponent  $\beta$  (from  $v \sim (f_0 - f_c)^\beta$ ) as  $\beta = 1/2$ . At finite temperature this sharp continuous

transition is smoothed and, at variance with the peculiar  $T = 0$  case, the problem becomes a non-trivial collective problem. In the following sections we discuss the thermally activated dynamics below the depinning threshold for  $|f_0 - f_c| \ll f_c$ , and then the subtle  $f_0 = f_c$  case at finite temperature.

## III. ACTIVATED DYNAMICS SCALING NEAR THE DEPINNING THRESHOLD

The finite temperature creep dynamics described by Eq.(1) well below  $f_c$  was studied in Ref. [42] using renormalization group methods. Here we want to calculate the value of  $v$  for finite temperature, and for  $f_0$  very close to  $f_c = 1$ . If  $f_0$  is only slightly below one, and  $T$  is very small ( $T \ll (f_c - f_0)$ ) the dynamics is dominated by thermal activation events in which patches of the interface (of linear size  $l_0$  to be determined below) advance a definite spatial amount. These patches then grow in size deterministically.

We consider a  $d$  dimensional system with periodic boundary conditions at very low temperature, and assume that we start with a nearly flat interface resting in a local minimum of the tilted potential  $[\sin(h) - f_0 h]$ , with  $f_0 = f_c - \varepsilon$ , and  $\varepsilon \ll 1$ . Then we can approximate the potential by  $\varepsilon h - h^3/6$  near the transition point [43]. The local energy minimum is thus located at  $h = -\sqrt{2\varepsilon}$ , the maximum at  $h = +\sqrt{2\varepsilon}$ . Using this expansion in Eq. (1) the resulting dynamical equations that will describe the escape from the energy minimum can be written in a normalized form as

$$\frac{\partial h(r, t)}{\partial t} = \frac{h^2}{2} - \varepsilon + \nabla^2 h + \sqrt{T}\eta(t, r). \quad (5)$$

We first calculate the rate of nucleation of defects  $R$  (that make the interface advance) per unit of time and unit of volume of the system, in a system with spatial extension  $L$ .  $R$  will depend on the two parameters  $T$  and  $\varepsilon$  present in Eq. (5) and also on  $L$ , i.e., we can write  $R(T, \varepsilon, L)$ . First we sketch a scaling analysis that allows to reduce the three-parameter dependence of  $R$  to a two-parameter dependence. Suppose we know the value of  $R$  for given values of  $T$ ,  $\varepsilon$  and  $L$ . Then we scale all variables and parameters in Eq. (5) according to the following table,

$$\varepsilon \rightarrow \tilde{\varepsilon} \equiv k\varepsilon \quad (6)$$

$$h \rightarrow \tilde{h} \equiv k^{1/2}h \quad (7)$$

$$t \rightarrow \tilde{t} \equiv k^{-1/2}t \quad (8)$$

$$r \rightarrow \tilde{r} \equiv k^{-1/4}r \quad (9)$$

$$L \rightarrow \tilde{L} \equiv k^{-1/4}L \quad (10)$$

$$T \rightarrow \tilde{T} \equiv k^{(6-d)/4}T \quad (11)$$

where  $k$  is an arbitrary scaling factor. It is readily verified that tilde variables satisfy an equation formally identical to the original one. The above scaling means that the

number of activation events in corresponding time and space intervals are equal for the original and the scaled equation. In concrete,

$$R(T, \varepsilon, L)[t][r]^d = R(\tilde{T}, \tilde{\varepsilon}, \tilde{L})[\tilde{t}][\tilde{r}]^d \quad (12)$$

or

$$R(T, \varepsilon, L) = R(k^{(6-d)/4} T, k\varepsilon, k^{-1/4} L) k^{-(d+2)/4} \quad (13)$$

Since  $k$  is arbitrary we can choose  $k \sim 1/\varepsilon$  to obtain

$$R(T, \varepsilon, L) = \varepsilon^{(d+2)/4} R\left(\frac{T}{\varepsilon^{(6-d)/4}}, 1, L\varepsilon^{1/4}\right) \quad (14)$$

Alternatively, and assuming for simplicity the large system size limit ( $L\varepsilon^{1/4} \gg 1$ ) we can accommodate the previous expression as

$$R(T, \varepsilon) = T^{\frac{d+2}{6-d}} \mathcal{F}\left(\frac{\varepsilon^{(6-d)/4}}{T}\right) \quad (15)$$

where we have dropped the  $L$  dependence and defined the unknown function  $\mathcal{F}$  as

$$\mathcal{F}(x) \equiv x^{\frac{d+2}{6-d}} R(1/x, 1, \infty) \quad (16)$$

Eq. (15) explicitly gives the two parameter form of  $R(T, \varepsilon)$  in terms of an unknown function  $\mathcal{F}$  of a single variable.

The combination  $\varepsilon^{(6-d)/4}/T$  in the argument of  $\mathcal{F}$  suggests that  $\varepsilon^{(6-d)/4}$  is actually a relevant energy scale of the problem and thus we will denote  $\alpha = (6-d)/4$  as the “energy exponent”. In fact, its physical meaning can be unveiled by a simple variant of the “droplet” argument [33, 44]. Suppose we want to estimate what is the optimal linear size  $l_0$  of a patch of the surface to jump the energy barrier implied by the force density term  $h^2/2 - \varepsilon$  in Eq. (5). Assuming simple excitations, solely characterized by its linear size  $l_0$  and displacement  $h$ , the additional elastic energy of order  $(h/l_0)^2 l_0^d$  must be added to the potential energy  $(\varepsilon h - h^3/6)l_0^d$ , yielding the patch energy near  $f_c$ ,

$$E(h, l_0) \sim (\varepsilon h - h^3/6)l_0^d + (h/l_0)^2 l_0^d/2 \quad (17)$$

For any  $0 < d < 6$  the excitation energy  $E(h, l_0)$  has an extremum at  $l_0^* \sim \varepsilon^{-1/4}$  and  $h^* \approx \sqrt{\varepsilon}$ , yielding the exact scaling result

$$E^* \equiv E(h^*, l_0^*) \sim \varepsilon^{(6-d)/4}. \quad (18)$$

This confirms the physical connection with Eq. (15). For  $d < 2$  such extremum is a saddle point and  $E^*$  is the minimal barrier to advance forward. The optimal size  $l_0^* \sim \varepsilon^{-1/4}$  is such that the small ( $l_0 \ll l_0^*$ ) frequently activated patches are futile (i.e. they are quickly reversed) while large enough ( $l_0 > l_0^*$ ) patches trigger irreversible forward jumps of the whole segment. This physical argument also makes clear that the function  $\mathcal{F}$  in Eq. (15)

will contain a dominant factor  $\exp(-C\varepsilon^{(6-d)/4}/T)$  corresponding to an Arrhenius factor for the activation of these kind of optimal patches, provided  $T \ll \varepsilon^{(6-d)/4}$  and under the assumption that the considered segment size is larger than  $l_0$  [45].

All the previous scaling analysis can be done also for a non-quadratic force minimum, replacing  $h^2 \rightarrow h^\gamma$  in the rhs of Eq. (5), yielding (see Appendix Sec.A),

$$R(T, \varepsilon) = T^{\frac{(\gamma-1)(d+2)}{2(\gamma+1)-(\gamma-1)d}} \mathcal{F}(\varepsilon^{2-\frac{(2+d)(\gamma-1)}{2\gamma}}/T) \quad (19)$$

in the limit of large sizes  $LT^{\frac{\gamma-1}{2\gamma-\gamma d+d+2}} \gg 1$ . Eq.(19) reduces to Eq. (15) for  $\gamma = 2$ . In particular it generalizes the energy exponent to  $\alpha = 2 - (2+d)(\gamma-1)/2\gamma$ . The above results are valid for estimating the thermally activated decay rate of an initially flat segment of the interface by the production of a single defect. We now analyze in more detail the simplest cases, namely the particle and the elastic string, keeping the standard  $\gamma = 2$  for simplicity.

### A. Single Particle

For a single particle ( $d = 0$ ) each activation event represents the jump over one barrier, and leads to the advance of the particle by a finite amount  $2\pi$ . This means that the velocity in the single particle case will follow the scaling:

$$v_{d=0}(\varepsilon > 0, T) \sim R_{d=0} \sim T^{1/3} \mathcal{F}(\varepsilon^{3/2}/T) \quad (20)$$

The explicit form of the function  $\mathcal{F}$  in Eq. (20) and then the form of  $v$  is in fact well known in the limit  $\varepsilon > 0$ ,  $T \ll \varepsilon^{3/2}$ , which is the thermally activated regime. This corresponds to the Kramers problem of escape over a barrier. The velocity is simply proportional to the inverse of the escape time of a thermal particle in the potential well  $\varepsilon h - h^3/6$ . Kramers’ formula applied to this case provides

$$v_{d=0}(T \ll \varepsilon^{3/2}) = \sqrt{\varepsilon} \exp\left(-\frac{4\sqrt{2}}{3} \frac{\varepsilon^{3/2}}{T}\right) \quad (21)$$

This expression satisfies the scaling expression Eq. (20).

In the present single particle case the scaling argumentation can be extended to negative (but small)  $\varepsilon$ , meaning  $f_0$  slightly above the critical value  $f_c = 1$ , since in this case the dynamics is also dominated by the bottlenecks near the points where  $v$  is very small. This means that Eq. (20) can also be used for  $\varepsilon < 0$ . In this case, there is a finite limit for the velocity as  $T \rightarrow 0$ , and for this to be the case  $f(-x) \sim (-x)^{1/3}$  for  $x \rightarrow \infty$ , leading to

$$v_{d=0}(\varepsilon < 0, T = 0) \sim (-\varepsilon)^{1/2} \quad (22)$$

which is the expected result. Eq. (20) used at  $\varepsilon = 0$

also indicates that for a single particle  $v_{d=0}(\varepsilon = 0, T) \sim T^\psi$ , with a well defined thermal rounding exponent  $\psi = 1/3$  [21, 46, 47].

## B. Elastic String

We now analyze the case  $d = 1$ , corresponding to an elastic string. Eq. (15) becomes in this case

$$R_{d=1}(T, \varepsilon) = T^{3/5} \mathcal{F}(\varepsilon^{5/4}/T) \quad (23)$$

In  $d = 1$  the relation between  $R$  and the velocity of the interface is as follows:  $R$  represents the rate of creation of kink/anti-kink pairs. Each pair contributes equally to the velocity, so the velocity is proportional to the number  $N$  of kink/anti-kink pairs present in the system. The equilibrium value of  $N$  is obtained by balancing the creation of kinks ( $\sim R$ ) to its annihilation rate, which (like a chemical reaction between two species) is proportional to  $N^2$  [48]. Namely

$$\frac{dN}{dt} \sim R - N^2 \quad (24)$$

By requiring equilibrium ( $dN/dt = 0$ ) we obtain

$$v \sim N \sim R^{1/2}. \quad (25)$$

Therefore,

$$v_{d=1}(T, \varepsilon) = T^{3/10} \mathcal{G}(\varepsilon^{5/4}/T) \quad (26)$$

where  $\mathcal{G} \equiv \sqrt{\mathcal{F}}$ . Alternatively we can also write

$$v_{d=1}(T, \varepsilon) = \varepsilon^{3/8} \mathcal{G}(\varepsilon^{5/4}/T) \quad (27)$$

In Fig. 1 we test these scalings numerically. As shown in Fig. 1(b) there is an excellent agreement below the depinning threshold, i.e., for  $\varepsilon > 0$ . One remarkable thing about the scaling of Eq. (26) is that it is *not* compatible with the well known behavior of  $v$  for negative  $\varepsilon$  (i.e.  $f_0 > 1$ ) and  $T = 0$ . In fact, if a  $T$ -independent limit is going to be extracted from Eq. (26) this should be  $v \sim (-\varepsilon)^{3/8}$ , that does not coincide with the known exact result  $v(T = 0, \varepsilon < 0) \sim (-\varepsilon)^{1/2}$ . This incompatibility can be appreciated in the  $\varepsilon < 0$  (i.e.,  $f > f_c$ ) part of Fig. 1(b), where clearly the curves do not collapse. The good collapse for  $f > f_c$  is obtained rescaling  $\varepsilon$  with the same energy exponent, namely  $\varepsilon/T^\alpha = (f - f_c)/T^\alpha$  with  $\alpha = (6 - d)/4 = 5/4$ , but using  $v/T^{2/5}$  in the vertical axis, in order to obtain  $\beta = 1/2$  (Fig. 1(c)). The conclusion is that a unique thermal rounding scaling is not valid in this problem for  $d$  equal to (or larger than) one. In particular, if we try to define a single thermal rounding exponent, we should choose  $\psi = 3/10$  from the  $\varepsilon > 0$  part of the scaling, but  $\psi = 2/5$  from the  $\varepsilon < 0$  part. We will see below how this incompatibility manifests in the true form of  $v(T)$  at  $\varepsilon = 0$  having a non-trivial

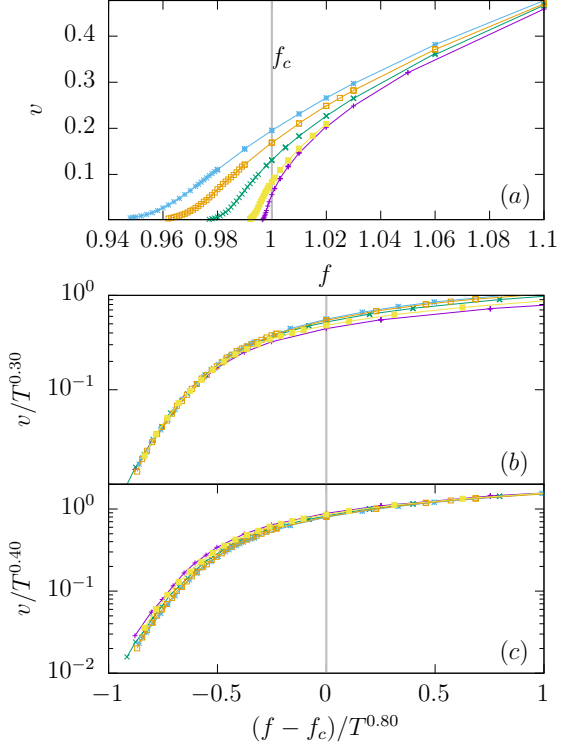


FIG. 1. Velocity force characteristics around the depinning threshold of an elastic string in the washboard potential, at different temperatures  $T = 0.003, 0.02, 0.03, 0.01, 0.001$  (a) Whole range around  $f_c = 1$ . Best scaling collapses just below the threshold  $f \lesssim f_c$  (b) and just above the threshold  $f \gtrsim f_c$  (c). The exponents are clearly different above and below threshold, in contrast with the one particle case.

logarithmic correction.

## IV. THERMAL ROUNDING OF THE DEPINNING TRANSITION

The results in Sec. III clearly show that a unique global scaling of the form

$$v = T^\psi \mathcal{F}(\varepsilon^\alpha/T) \quad (28)$$

is valid only for the simplest case of a single particle, but does not apply to interfaces in finite dimensions.

For an extended interface the form of the activated dynamics scaling below  $f_c$  ( $\varepsilon > 0$ ) cannot be extrapolated to the  $\varepsilon < 0$  region. Moreover, the form of the velocity as a function of temperature predicted by Eq.(28) when  $\varepsilon = 0$ , namely

$$v \sim T^\psi \quad (29)$$

is not accurately satisfied, as we will show below. It turns out that this scaling has important logarithmic corrections that we will now address.

We will make a detailed analysis of the dynamics of the

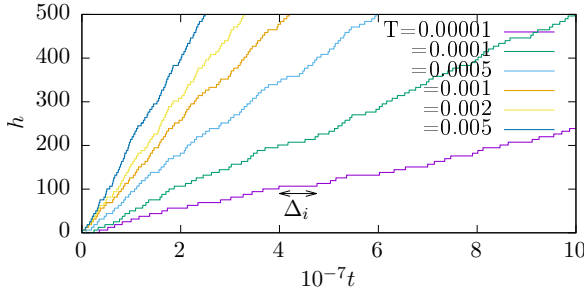


FIG. 2. Position-time plot for a single particle at the critical force, at different temperatures, as indicated. The motion proceeds by a sequence of jumps of size  $2\pi$  separated by stochastic waiting times  $\Delta_i$ .

system right at the critical force  $f_c$  (i.e.  $\varepsilon = 0$ ). Thus the model to be studied is that of Eq. (1) for a sinusoidal pinning potential at the critical force, namely

$$\frac{\partial h(r, t)}{\partial t} = -\cos(h) + 1 + \nabla^2 h + \sqrt{T}\eta(t, r), \quad (30)$$

as a function of temperature, in the  $T \ll 1$  limit, where critical scaling functions and exponents are expected.

### A. Single Particle

To serve as a reference we start with the analysis of the single particle case, that is, solving

$$\frac{dh}{dt} = -\cos(h) + 1 + \sqrt{T}\eta(t), \quad (31)$$

with  $\langle \eta(t)\eta(t') \rangle = \delta(t - t')$ . Fig. 2 displays the numerically obtained evolution of  $h(t)$  for different temperatures. We clearly see that the dynamics proceeds through abrupt jumps between successive “bottlenecks” positions that occur when  $h$  is a multiple of  $2\pi$ , at which the particle spends most of the time. These are the points at which the deterministic force on the particle vanishes. The average velocity as a function of temperature follows the prediction of Eq. (20) at  $\varepsilon = 0$ , namely  $v \sim T^{1/3}$ . However we emphasize that this scaling applies not only to the average velocity (which is related to the average waiting time at the bottlenecks) but also to the whole distribution of time intervals spent at the bottleneck positions. This is shown in Fig. 3(a) where the cumulative probability distribution  $F(\Delta, T)$  of the time intervals  $\Delta$  spent at each bottleneck is calculated for different small temperatures [49]. As shown in Fig. 3(b) the results adjust perfectly to the scaling law

$$F(\Delta, T) = F_0(\Delta/T^{1/3}) \quad (32)$$

Therefore, for the average particle velocity  $v \sim \overline{\Delta^{-1}}$  we get  $v \sim T^{1/3}$ , as it has been observed with high accuracy (see for instance Ref. 21, and Fig. 20). This simply

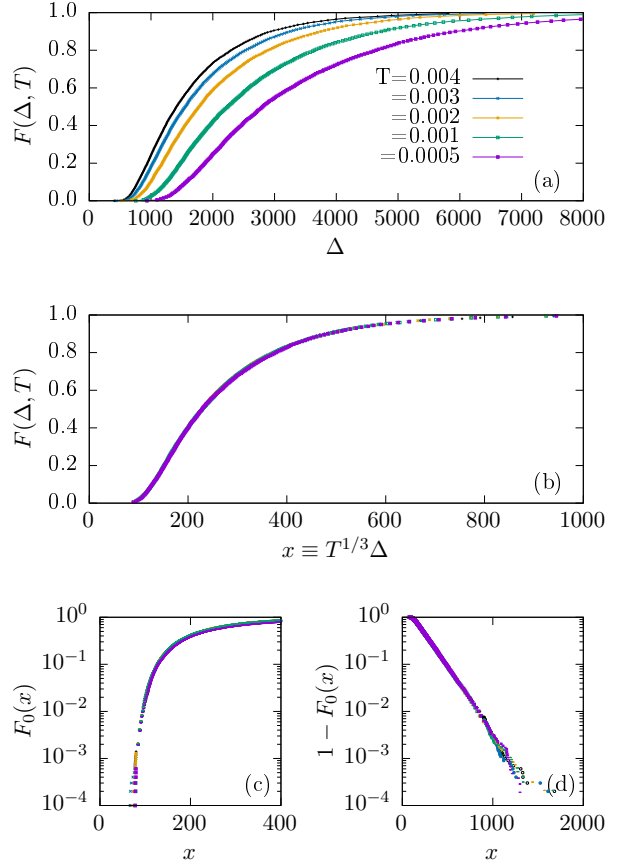


FIG. 3. (a) Cumulative distribution [ $F(\Delta, T) \equiv \text{Prob}(\Delta_i < \Delta)$ ] of the stochastic waiting times  $\Delta_i$  (see Fig. 2) between successive jumps of a single particle ( $d = 0$ ) in a tilted washboard potential, exactly at  $f = f_c$ , for different temperatures. (b) The distribution can be collapsed onto a single curve by plotting it as a function of  $T^{1/3}\Delta$ . The left (c) and right (d) tails of the cumulative distribution highlight, respectively, the slower-than-exponential growth of the probability for short waiting times and its exponential decay for large waiting times.

confirms that the particle accurately obeys the thermal rounding scaling of Eq. (29).

As shown in Fig. 3(c) and (d),  $F_0(\Delta)$  displays an exponential decay at large  $\Delta$  and a sort of “pseudogap” at small  $\Delta$ , where  $F_0(T^{1/3}\Delta)$  is almost zero. The existence of this “minimum time” for a jump [50] will play an important role in the analysis of the movement of the one-dimensional string, that we consider in the following.

### B. Elastic String

#### 1. Kink/anti-kink dynamics at $f = f_c$

To gain insight in the form in which a one-dimensional elastic string moves at  $f = f_c$ , we solve numerically Eq.

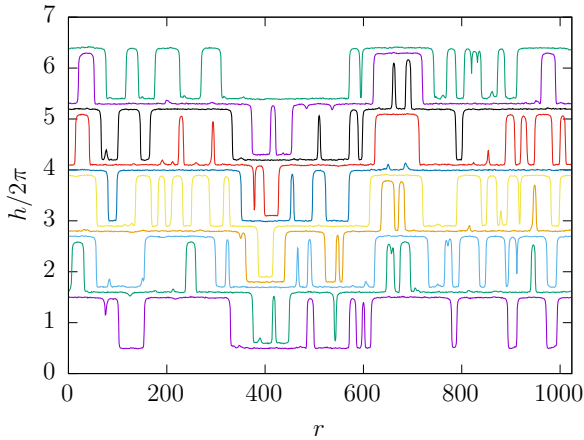


FIG. 4. A sequence of numerically generated configurations  $h(r, t)$  for an elastic string of size  $L = 1024$ ,  $T = 5 \times 10^{-5}$ , exactly at the critical force  $f_c = 1$ . Consecutive configurations at increasing times (from bottom to top) have been differently colored and slightly shifted vertically by  $\sim 0.1$  for clarity.

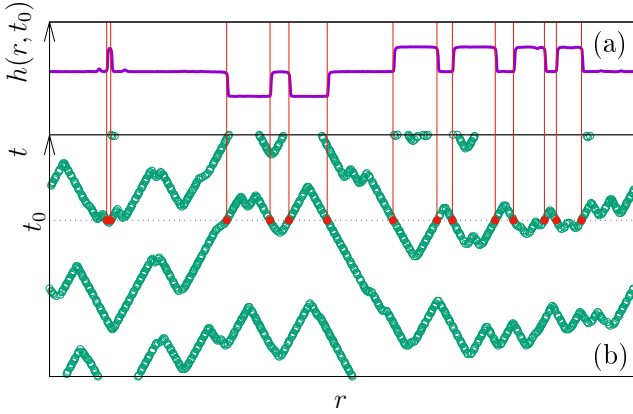


FIG. 5. (a) Snapshot of a configuration  $h(r, t_0)$  of the interface at  $t = t_0$ , exactly at the critical force  $f_c = 1$  and  $T = 10^{-5}$ , generated from Eq. (30) for  $L = 1024$ . (b) Kink trajectories in space-time. Red dots correspond to kink positions at  $t = t_0$ . Dashed vertical lines show their correspondence with  $h(r, t_0)$  kinks.

(30) for  $d = 1$  by finite differencing using the stochastic Euler method on  $L$  elastically coupled particles. In Fig. 4 we display a few snapshots of the configuration of the system in a well equilibrated state, at slightly increasing times. We see a characteristic structure in which pieces of the interface are located at positions corresponding to the bottlenecks of the potential. For convenience we will number successive bottlenecks with an integer index  $\nu$ , such that the interface stays at  $h = 2\pi\nu$ . Different pieces of the interface are connected through “kinks” in which the interface passes from  $\nu$  to  $\nu \pm 1$ , as again shown in Fig. 5(a). It is important to realize that the kinks move in a very deterministic and predictable way. In fact, as a piece of interface at position  $\nu$  has a potential energy per site of

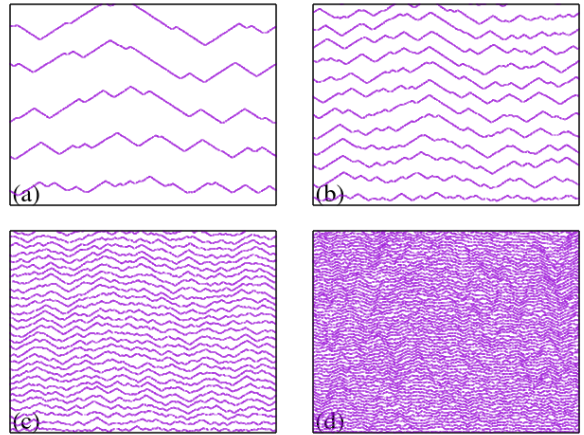


FIG. 6. Numerically generated kink trajectories exactly at the critical force for different temperatures,  $T = 10^{-6}$  (a),  $T = 10^{-5}$  (b),  $T = 10^{-4}$  (c), and  $T = 10^{-3}$  (d), for a string of size  $L = 1024$ . The vertical and horizontal directions are time and position respectively, and have the same extent in the four panels.

$-2\pi\nu$ , a kink connecting  $\nu$  and  $\nu + 1$  decreases its energy by moving in the direction that increases the extent at  $\nu + 1$  and decreases that at  $\nu$ . This produces that all kinks in the system move at a constant velocity  $c \approx f_c \xi / 2\pi$ , where  $\xi$  is the kink width [51]. For our numerical setup (Eq. (30)) we find  $c \approx 0.24$ , in consistence with  $f_c = 1$  and the observed  $\xi \approx O(1)$  (see Fig. 4), always in the direction of producing a net advance of the interface. As kinks move always at the velocity  $\pm c$ , they travel along straight lines of constant slope when plotted in a position-time graph as shown in Fig. 5(b). As kink and anti-kinks collide, they annihilate at the “ $\Lambda$ ”-shaped points. In addition, kink/anti-kink pairs nucleate at the “ $V$ ”-shaped points. Note that the space-time plot of Fig. 5(b) is a full picture of the dynamics of the string in spatial scales larger than the typical size of the kinks.

In Fig. 6 we can qualitatively appreciate the kink dynamics at  $f = f_c$  for different temperatures in the steady-state. The four panels correspond to four different increasing temperatures. The space and time extent of the four panels is the same. We observe in particular that the slope of the straight segments (corresponding to kink propagation) has the same value  $c^{-1}$  for all temperatures. The space-time segments describing kink trajectories form a well defined sequence of sawtooth lines percolating space but separated by distinguishable time-gaps (i.e., different lines do not get close vertically in practice). It is worth stressing however that, in spite of these time gaps, the one dimensional interface at the steady-state is actually never completely trapped in a metastable state: for given time  $t$  a large enough interface always has pairs of kinks evolving quasi-deterministically. In other words, a line with  $t = \text{cte}$  in space-time always cuts the trajectory of some kinks. Another interesting property that can be appreciated in the Fig. 6 is that increasing tem-

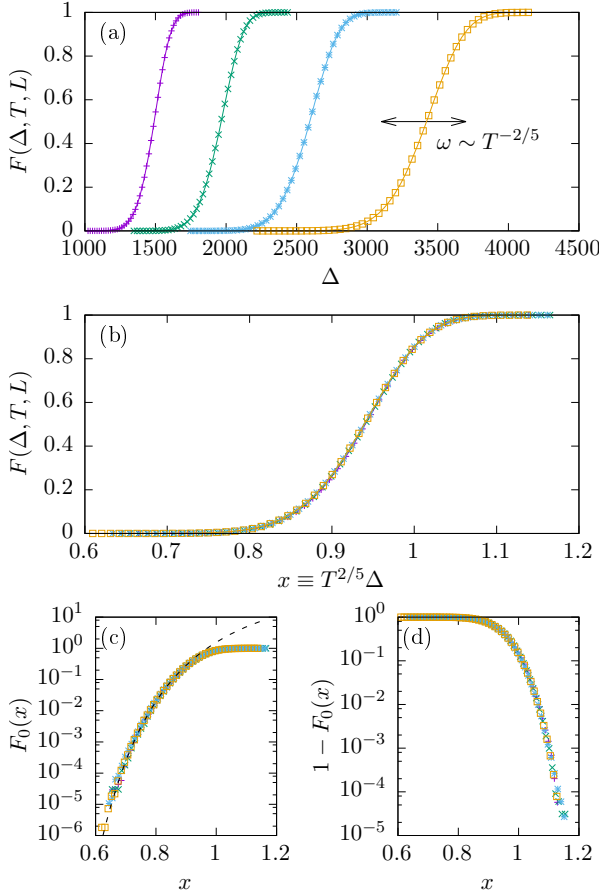


FIG. 7. Waiting-time cumulative distributions for the activation of the first pair of kinks in a flat ( $d = 1$ ) elastic string exactly at  $f = f_c$ , for different temperatures  $T$  and string sizes  $L$ , such that  $TL^{1/5} = \text{cte}$ . (a) The rightmost curve corresponds to  $L = 2^{16}, T = 1.25 \times 10^{-9}$ , each following curve to the left doubles the temperature. (b) Master curve using the time-temperature-length scaling,  $F(\Delta, T, L) \sim F(T^{2/(6-d)} \Delta, TL^{1/(6-d)}) \equiv F_0(T^{2/(6-d)} \Delta)$  in the case  $d = 1$ . (c) The dashed line  $\sim \exp[-4.58/x^3]$  is an empirical fit of the left part of  $F_0(x)$ . (d) Detail of the right tail of  $F_0(x)$ , to be compared with the single particle case in Fig. 3.

perature increases both the space-time density of annihilation and creation events, and decreases the time gaps, strongly suggesting a space-time-temperature scaling relation, that we will discuss in detail.

In Sec. III, and working below the critical force, we considered the nucleation of kink/anti-kink pairs to occur at a rate  $R$  that was simply a function of temperature. This led to the estimation that the velocity interface is  $v \sim R^{1/2}$  (Eq. (25)). This analysis was appropriate because in that case there was a finite energy barrier to be surmounted, and the dynamics of this activation is statistically a Poisson process: if an attempt to climb the barrier has failed, the next one has to start over, independently of how many previous attempts have been

made. But right at  $f_c$ , the transition between successive bottleneck position does not require the climbing of any energy barrier. The bottlenecks are characterized by a flat potential in which the deterministic force vanishes, and the transition time displays the typical time gap already seen in the single particle case (Fig. 3). In fact, in Fig. 7 we present the same analysis of Fig. 3 but for the case of the elastic line. Here we start in a flat configuration of a system of size  $L$  (with periodic boundary conditions) at temperature  $T$  and look for the first time a kink/anti-kink pair is observed. Fig. 7(a) shows the cumulative distribution function  $F$  of the first nucleation time  $\Delta$ , for different temperatures  $T$  and system sizes  $L$ . In panel (b) the same data are shown to collapse onto a single curve when  $F$  is plotted against  $T^{2/5} \Delta$  for a fixed  $L^{1/5} \Delta \equiv \text{cte}$ . This scaling follows immediately (using  $d = 1$ ) from the analysis in Section III, that produces

$$F(\Delta, T, L) = F_0(T^{2/(6-d)} \Delta, T^{1/(6-d)} L). \quad (33)$$

Since we are fixing  $LT^{1/5}$ , for simplicity we will omit the  $L$  dependence everywhere and simply write  $F(\Delta, T, L) = F_0(x)$  with  $x \equiv T^{2/5} \Delta$  and  $F_0(x)$  the master curve. It is interesting to compare the tails of  $F_0(x)$  for the string and the particle. In the single particle case  $F_0(x)$  is exponential for large  $x$ , while the elastic string displays a clear faster-than-exponential decay at large  $x$ . On the other hand for small  $x$ , both cumulative distributions display a slower than exponential growth.

The results in Fig. 7 clearly display the “gap” effect in the nucleation time (also observed for the single particle case in Fig. 3), pointing also to the fact that this nucleation cannot be considered anymore (as it was in the activated regime) a Poisson process. Thus the probability to nucleate a kink/anti-kink pair in a piece of interface at  $\nu$  depends on how much time the surface has stayed at  $\nu$  already. To get an idea of this phenomenon and its importance, it is worth looking again in Fig. 6 to the ubiquitous time-gaps appearing in sequences of many branches for different temperatures. The rather well defined values of the vertical gaps between different branches in the plot in Fig. 6 is a consequence of the fact that nucleation time cannot be arbitrarily small, as seen also in Fig. 7.

## 2. $v(T)$ curve at $f = f_c$

Armed with the qualitative understanding of the dynamic we gained in the previous section (Sec. IV B 1), we can address quantitatively the expected form of the temperature dependence of the velocity  $v$  right at  $f_c$ , namely the thermal rounding law. Referring to the plots in Fig. 6, the value of  $v$  is nothing more than  $2\pi$  divided by the average temporal separation between successive branches. We must estimate this average temporal separation in order to calculate  $v$ .

The overall form of the  $v(T)$  curve will emerge as a

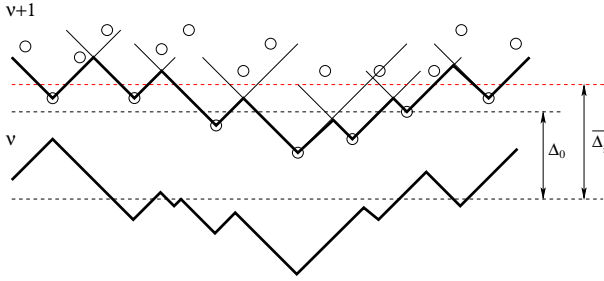


FIG. 8. Sketch of the space-time configuration of an interface showing branches  $\nu$  and  $\nu + 1$ . The red dotted line is the average temporal position of all circles. True  $\nu + 1$  branch occurs on average at an early time and shows the effects of the propagating kinks.

combination of two effects: one is the intrinsic nucleation time of kink/anti-kinks as given in Fig. 7; the other is the effect of kink/anti-kink propagation in the system. Let us consider the sketch of Fig. 8 depicting the branch  $\nu$  in the position-time plot, from which we want to calculate the  $\nu + 1$  branch. In Fig. 8 we consider that each horizontal position represents a piece of the interface, of size at least the lateral size of kinks. This means that it makes sense to consider that there will be a typical, intrinsic time for the nucleation of a kink/anti-kink pair at any horizontal position in Fig. 8. These intrinsic times  $\Delta_i$  have to be drawn from the appropriate distribution in Fig. 7, and a typical realization is indicated in Fig. 8 through the open circles. If the  $\nu + 1$  branch was composed simply by the collection of circles, the average time separation between branches  $\nu$  and  $\nu + 1$  would be simply  $\bar{\Delta}_i$ , i.e., the average value of  $\Delta_i$ , over all  $i$ . However, each circle propagates a “forward light cone” corresponding to the time evolution of potentially nucleating kink/anti-kink pairs. The lower envelope of all these cones will be the actual  $\nu + 1$  branch in the system. We see the average time shift  $\Delta_0$  for the true  $\nu + 1$  branch is smaller than  $\bar{\Delta}_i$ .

In order to calculate  $\Delta_0$  we notice that the branch  $\nu + 1$  is composed by pieces of the cones corresponding to the lowest values of the nucleation times at all sites, or in other words the lowest circles in Fig. 8. If  $M$  is the average number of sites affected by a single cone, the typical value of  $\Delta_0$  corresponds to the typical value of the minimum of  $M$  variables  $\Delta_i$  with cumulative distribution  $F(\Delta, T)$ , the function plotted in Fig. 7. This minimum is roughly given by the condition

$$MF(\Delta_0, T) = 1, \quad (34)$$

and the velocity of the interface will be given by  $v = 2\pi/\Delta_0$ . The main temperature dependence of  $v$  comes from the temperature dependence of  $F(\Delta_0, T)$ . The velocity dependence of  $M$  will account for a logarithmic correction, as we will now see. From the numerical results in Fig. 7(c),  $F(\Delta_0, T)$  can be very well approximated

(particularly when  $F \ll 1$ ) as

$$F(\Delta_0, T) \simeq \exp(-C/(T^{2/5}\Delta_0)^3) \quad (35)$$

with  $C \simeq 4.58$  a numerical constant. Note that the form of the combination  $T^{2/5}\Delta$  comes already from the scaling of time and temperature, in the analysis of Section III applied to the  $d = 1$  case, which is also valid for  $\varepsilon = 0$  as it is the case here. The third power instead, is just a rough numerical fitting (see dashed-line in Fig. 7(c)). The dependence of  $M$  on temperature is roughly given by the following argument: a cone starting at one of the lowest circles in Fig. 8 will be part of the  $\nu + 1$  branch for a number of sites  $M$ , such that  $M/c \sim \omega$ , where  $\omega$  is the width of the  $F(\Delta, T)$  function. According to Eq. (35) it scales with temperature as  $\omega \sim T^{-2/5}$ . Putting the pieces together, and since  $c$  is just a constant, this gives simply

$$M \sim T^{-2/5} \quad (36)$$

Using now Eqs. (35) and (36) in Eq. (34) we finally obtain

$$v = c_1 T^{2/5} [-\log(c_2 T)]^{1/3} \quad (37)$$

where we have dug into  $c_1$  and  $c_2$  all unknown constants of the analysis. In general dimension  $d$ , the kink-antikink pair of the  $d = 1$  case is replaced by a  $(d-1)$ -dimensional domain wall describing a droplet boundary, allowing  $d$ -dimensional patches to advance from one branch to the following in an isotropic way. The mechanism just described of nucleation, expansion and coalescence of cones qualitatively applies in general dimension and the expected form of  $v$  at  $f_c$  is

$$v = c_1 T^{\frac{2}{(6-d)}} [-\log(c_2 T)]^\delta \quad (38)$$

where the exponent  $\delta$  of the logarithmic correction is 0 in  $d = 0$ , and  $1/3$  in  $d = 1$ . For  $d > 1$  we expect it to be different from zero, but we have not attempted a precise determination.

The result we have obtained for the dependence of  $v(T)$  shows a main power law dependence but also an important logarithmic correction that can have an important effect on experimentally observed values. Qualitatively, the origin of the two parts can be traced back to the particular dynamics of the problem. The  $T^{2/(6-d)}$  factor in the velocity comes from the average transition time between bottleneck configurations at which the interface spends most of the time. The logarithmic factor is a consequence of the linear-in-time increase of the extent of the interface at position  $\nu$  before nucleating the defect that will allow the transition to the  $\nu + 1$  position.

We now check the form of  $v(T)$  from Eq. (37) against numerical simulations. Fig. 9(a) show the results of a simulation in the full model at  $f = f_c$ . If we were trying to fit a power law, we would probably fit an exponent

$\simeq 0.38$  (yellow line) at least in the left part of the figure. Yet, our expected behavior (Eq. (37)) produces a more satisfactory and consistent result. By fitting appropriately  $c_1$  and  $c_2$  we find the green curve, that fits the data in a much broader range of temperatures. This is even clearer in panel (b) where an effective power-law exponent as a function of temperature is obtained  $\psi_{\text{eff}} \approx d \log v / d \log T$ , using the method of consecutive slopes, and fitting pure power-law in windows of size  $[T - \Delta T, T + \Delta T]$  with  $\log((T + \Delta T)/(T - \Delta T)) = 3$ . This effective exponent shows a dependence compatible with very slow convergence to 0.4 when  $T \rightarrow 0$ , as Eq. (37) implies. Also, in panel (c) the data are plotted in such a way that they must follow a straight line if Eq. (37) is followed. We see in fact that they follow very well this behavior, except for large temperatures in which some effects not considered in our analysis enter into play (particularly when temperature becomes a sizeable fraction of the total amplitude of the corrugation potential and the system crossovers to the fast-flow regime where  $v \sim f_c$ ).

## V. CONCLUSIONS

The naive analogy of the depinning transition with standard phase transitions suggests that the average velocity of an extended elastic manifold exactly at the threshold should scale as  $v \sim T^\psi$  for small temperatures  $T$ , with  $\psi$  the thermal rounding exponent. Pioneer arguments testing this idea, and yielding the first non-trivial predictions for  $\psi$ , were first given in the context of charge density wave models with quenched disorder [19, 22, 52] and later proposed for models of disordered elastic interfaces. In particular, they led to the relation  $\psi = \beta/\alpha$ , with  $\beta$  the zero temperature velocity exponent ( $v(f, T = 0) \sim (f - f_c)^\beta$ ) and  $\alpha$  the barrier exponent describing how barriers for nucleation of forward moving modes vanish approaching the depinning threshold from below ( $U(f) \sim (f_c - f)^\alpha$ ). In spite of several subsequent analytical [26, 53, 54], numerical [20, 21, 29, 55–58] (some of them with different predictions for  $\psi$ ) and experimental [20, 59, 60] studies, a proper understanding of the thermal rounding of the depinning transition seems to remain elusive.

We have analyzed a simple version model of the depinning transition, namely the interface in a washboard potential, and found that right at the threshold the velocity follows by Eq.(38), which contains an important logarithmic correction (when  $d \neq 0$ ) compared with the pure power-law behavior. We have shown that the logarithmic correction in this model can be physically explained in terms of a competition between the droplet nucleations (bounded by a kink-antikink pair in  $d = 1$  or a  $d - 1$  dimensional domain wall for  $d > 1$ ) and the expanding deterministic motion they immediately trigger. In either case the later deterministic motion is hence not only responsible for displacing pieces of the interface one

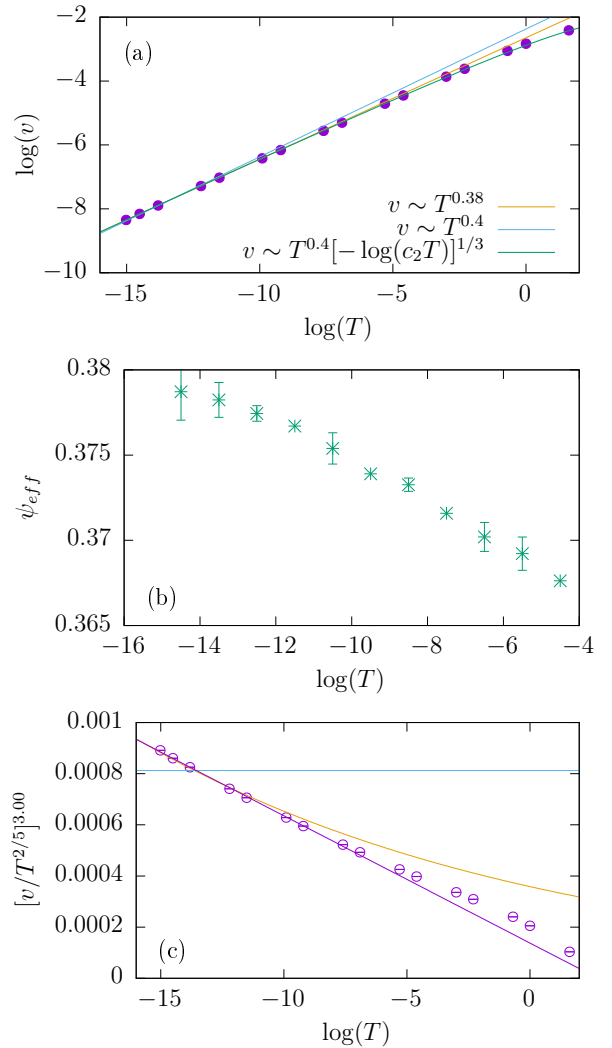


FIG. 9. (a) Velocity as a function of temperature ( $T \in [10^{-7}, 10]$ ) at  $f = f_c$ , for an elastic string of size  $L = 8388608$ . The yellow line is a naive pure power-law fitting of the form  $v \simeq T^{\psi_0}$ ,  $\psi_0 \simeq 0.38$ . The green line is a fit from our Eq. (37), consisting in a power law  $T^{2/(6-d)} = T^{0.4}$  multiplied by a logarithmic correction. The blue line, with slope  $2/(6-d) = 0.4$ , is used only for reference. (b) Effective power-law exponent  $\psi_{\text{eff}} \approx d \log v / d \log T$ , using the method of consecutive slopes (see text). (c) The same results as in (a) but plotted as  $[v/T^{0.4}]^3$  vs  $\log T$ , highlighting the logarithmic corrections. The accuracy of Eq. (37) is very good, except for large temperatures where some non-considered effects enter into play.

period further but also responsible for the deactivation of the nucleation in nearby sites (See Fig.8). It is worth stressing that the left tail of the waiting time distribution for nucleation plays a fundamental role in producing logarithmic corrections. At this respect we note that the characteristic space-time structure we observe at the depinning transition (see Fig 6) is clearly different from the one observed in the poly-nuclear growth model [61] (and other similar solid-on-solid growth models) where droplet

nucleations are randomly sampled from a Poisson distribution before expanding them. As shown in Fig. 7, a Poisson distribution does not apply at all to the thermally assisted dynamics at the critical force. Interestingly, the exponent  $2/(6-d)$  in Eq.(38) still agrees exactly with the relation  $\psi = \beta/\alpha$  (with  $\beta = 1/2$  and  $\alpha = (6-d)/4$ ) proposed in Ref. 22. Furthermore, we have shown that the same prefactor exponent  $\beta/\alpha$  actually holds for an infinite family of periodic potentials with different values of  $\alpha$  and  $\beta$  (Section A). Our results hence predict that, in practice, the effective thermal rounding exponent will approach  $\beta/\alpha$  slowly and from below in the limit of small temperatures.

Based on the above findings, we conjecture that the thermal rounding of the depinning transition in the more generic case of interfaces in disordered pinning landscapes for  $d > 0$  also displays logarithmic corrections, which may be written as

$$v = c_1 T^{\beta/\alpha} [-\log(c_2 T)]^\delta \quad (39)$$

where  $\delta > 0$  is a new exponent describing the left tail (or “pseudogap”) of the waiting time distribution for nucleation of localized modes exactly at the critical force. Such modes may be related to the marginally stable localized (at the Larkin length scale) soft modes found at the critical depinning configuration [62]. In this scenario, the deterministic expansion of thermally nucleated droplets  $d = 1$  in the toy model would be replaced by the analogous avalanche motion observed near the depinning threshold. Noteworthy, some interface models with disorder gave already evidence of logarithmic corrections [21]. Testing this conjecture more broadly may help to advance our understanding of the thermal rounding of the depinning transition of elastic manifolds.

## ACKNOWLEDGMENTS

We acknowledge discussions with S. Bustingorry and E. Ferrero. ABK also acknowledges V. Lecomte. PICT2016-0069 (MinCyT) y UNCuyo2019-06/C578.

## Appendix A: Generalization of the nucleation rate scaling

Here we consider the motion of a flat interface segment near the depinning transition ( $f = f_c - \varepsilon$ ) using a more general form for the bottleneck at  $h = 0$ ,

$$\frac{\partial h(r)}{\partial t} = h^\gamma - \varepsilon + \nabla^2 h + \sqrt{T} \eta(t, r) \quad (A1)$$

with  $\gamma$  characterizing the normal form of the periodic force  $-V'(h) \approx -h^\gamma$  around  $h = 0$  and all its periodic images. Using the same arguments leading to 11 we now arrive to its generalization,

$$\varepsilon \rightarrow \tilde{\varepsilon} \equiv k\varepsilon \quad (A2)$$

$$h \rightarrow \tilde{h} \equiv k^{\frac{1}{\gamma}} h \quad (A3)$$

$$t \rightarrow \tilde{t} \equiv k^{\frac{1}{\gamma}-1} t \quad (A4)$$

$$z \rightarrow \tilde{z} \equiv k^{\frac{1-\gamma}{2\gamma}} z \quad (A5)$$

$$T \rightarrow \tilde{T} \equiv k^{2-\frac{(2+d)(\gamma-1)}{2\gamma}} T \quad (A6)$$

which reduces for  $\gamma = 2$  to Eq. (11). Repeating the same steps than for  $\gamma = 2$  we obtain the generalized  $\gamma$  dependent nucleation rate per unit volume

$$R(T, \varepsilon, L) = \varepsilon^{\frac{(2+d)(\gamma-1)}{2\gamma}} R(T/\varepsilon^{2-\frac{(2+d)(\gamma-1)}{2\gamma}}, 1, LT^{\frac{\gamma-1}{2\gamma-\gamma d+d+2}}). \quad (A7)$$

Alternatively, for large sizes  $LT^{\frac{\gamma-1}{2\gamma-\gamma d+d+2}} \gg 1$ , we can write

$$R(T, \varepsilon) = T^{\frac{(\gamma-1)(d+2)}{2(\gamma+1)-(\gamma-1)d}} \mathcal{F}(\varepsilon^{2-\frac{(2+d)(\gamma-1)}{2\gamma}}/T) \quad (A8)$$

with  $\mathcal{F}(x)$  a master function,

$$\mathcal{F}(x) \equiv x^{\frac{(\gamma-1)(d+2)}{2(\gamma+1)-(\gamma-1)d}} R(1/x, 1, \infty) \quad (A9)$$

At  $T = 0$  is easy to see that the velocity at the depinning transition in this family of periodic potentials is  $v \sim (f - f_c)^\beta$  with  $\beta = 1 - 1/\gamma$ , since the problem reduces to the particle case [21]. If we use that  $\psi \approx \beta/\alpha$  we find the thermal rounding exponent  $\psi = \frac{2\gamma-2}{2\gamma-\gamma d+d+2}$ . In  $d = 1$  we get in particular  $\psi = \frac{2\gamma-2}{\gamma+3}$ , so for  $\gamma = 2$  we have  $\psi = \frac{2}{5}$ .

In Fig. 10 we compare with  $v$  data at  $f_c = 1$ , vs temperature  $T$ . As can be appreciated in Fig. 10(a) the ansatz  $\psi = \frac{2\gamma-2}{2\gamma-\gamma d+d+2}$  works reasonably, but corrections to the pure law scaling manifest already for temperatures  $T > 10^{-4}$  (in units of the microscopic energy scale which we have set to unity). Interestingly, as shown in Fig. 10(b), these corrections are accentuated for larger  $\gamma$ , corresponding to shallower bottlenecks  $h^\gamma - \varepsilon$  around  $h = 0$ . As we have discussed for  $\gamma = 2$  case, logarithmic corrections are originated in the strong suppression of the probability of small nucleation times. The enhancement of corrections for increasing values of  $\gamma$  indicates stronger gaps in the waiting time distributions.

[1] J. Ferré, P. J. Metaxas, A. Mougin, J.-P. Jamet, J. Gorron, and V. Jeudy, *Comptes Rendus Physique* **14**, 651

(2013), disordered systems / Systmes désordonnés.  
[2] W. Kleemann, *Annual Review of Materials Research* **37**,

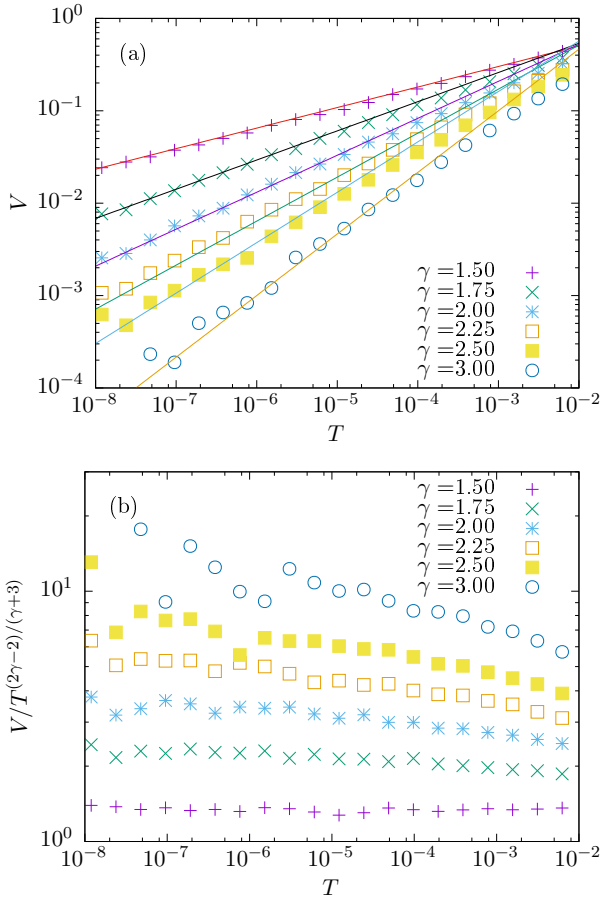


FIG. 10. (a) Velocity vs temperature at the depinning transition for an elastic string ( $d = 1$ ) of size  $L = 132768$  in a periodic potential characterized by the normal form exponent  $\gamma$ . Larger  $\gamma$  imply shallower force minima (see text). Lines display the power-law behavior  $v \sim T^{\psi(\gamma, d)}$ , where  $\psi = \frac{2\gamma-2}{2\gamma-\gamma d+d+2}$ . (b) Same data but highlighting the corrections to the power-law.

415 (2007).

- [3] P. Paruch and J. Guyonnet, *Comptes Rendus Physique* **14**, 667 (2013), disordered systems / Systmes dsordonnns.
- [4] D. Bonamy, S. Santucci, and L. Ponson, *Phys. Rev. Lett.* **101**, 045501 (2008).
- [5] L. Ponson, *Phys. Rev. Lett.* **103**, 055501 (2009).
- [6] C. Le Priol, J. Chopin, P. Le Doussal, L. Ponson, and A. Rosso, *Phys. Rev. Lett.* **124**, 065501 (2020).
- [7] J. F. Joanny and P. G. de Gennes, *The Journal of Chemical Physics* **81**, 552 (1984).
- [8] S. Moulinet, A. Rosso, W. Krauth, and E. Rolley, *Phys. Rev. E* **69**, 035103 (2004).
- [9] P. L. Doussal, K. J. Wiese, S. Moulinet, and E. Rolley, *EPL (Europhysics Letters)* **87**, 56001.
- [10] E. A. Jagla and A. B. Kolton, *Journal of Geophysical Research: Solid Earth* **115** (2010).
- [11] E. A. Jagla, F. P. Landes, and A. Rosso, *Phys. Rev. Lett.* **112**, 174301 (2014).
- [12] M. Tinkham, *Introduction to Superconductivity*, 2nd ed. (Dover Publications, 2004).
- [13] A. Pérez-Junquera, V. I. Marconi, A. B. Kolton, L. M.

Álvarez-Prado, Y. Souche, A. Alija, M. Vélez, J. V. Anguita, J. M. Alameda, J. I. Martín, and J. M. R. Parrondo, *Phys. Rev. Lett.* **100**, 037203 (2008).

- [14] V. I. Marconi, A. B. Kolton, J. A. Capitán, J. A. Cuesta, A. Pérez-Junquera, M. Vélez, J. I. Martín, and J. M. R. Parrondo, *Phys. Rev. B* **83**, 214403 (2011).
- [15] P. J. Metaxas, P.-J. Zermatten, R. L. Novak, S. Rothart, J.-P. Jamet, R. Weil, J. Ferr, A. Mougin, R. L. Stamps, G. Gaudin, V. Baltz, and B. Rodmacq, *Journal of Applied Physics* **113**, 073906 (2013), <https://doi.org/10.1063/1.4792216>.
- [16] D. S. Fisher, *Physics Reports* **301**, 113 (1998), [cond-mat/9711179](https://doi.org/10.1016/S0370-1573(97)00117-9).
- [17] M. Kardar, *Physics Reports* **301**, 85 (1998), [cond-mat/9704172](https://doi.org/10.1016/S0370-1573(97)00117-9).
- [18] S. Brazovskii and T. N., *Advances in Physics* **53**, 177 (2004), <https://doi.org/10.1080/00018730410001684197>.
- [19] D. S. Fisher, *Phys. Rev. B* **31**, 1396 (1985).
- [20] S. Bustingorry, A. B. Kolton, and T. Giamarchi, *Phys. Rev. E* **85**, 021144 (2012).
- [21] V. H. Purrello, J. L. Iguain, A. B. Kolton, and E. A. Jagla, *Phys. Rev. E* **96**, 022112 (2017).
- [22] A. A. Middleton, *Phys. Rev. B* **45**, 9465 (1992).
- [23] P. Le Doussal, K. J. Wiese, and P. Chauve, *Phys. Rev. B* **66**, 174201 (2002).
- [24] A. Rosso, P. Le Doussal, and K. J. Wiese, *Phys. Rev. B* **75**, 220201 (2007).
- [25] P. Le Doussal and K. J. Wiese, *Phys. Rev. E* **79**, 051106 (2009).
- [26] P. Chauve, T. Giamarchi, and P. Le Doussal, *Phys. Rev. B* **62**, 6241 (2000).
- [27] A. B. Kolton, A. Rosso, T. Giamarchi, and W. Krauth, *Phys. Rev. Lett.* **97**, 057001 (2006).
- [28] A. B. Kolton, A. Rosso, T. Giamarchi, and W. Krauth, *Phys. Rev. B* **79**, 184207 (2009).
- [29] E. E. Ferrero, S. Bustingorry, A. B. Kolton, and A. Rosso, *Comptes Rendus Physique* **14**, 641 (2013), disordered systems / Systmes dsordonnns.
- [30] P. M. Chaikin and T. C. Lubensky, *Principles of Condensed Matter Physics* (Cambridge University Press, Cambridge, 1995).
- [31] T. Hwa, M. Kardar, and M. Paczuski, *Phys. Rev. Lett.* **66**, 441 (1991).
- [32] A.-L. Barabsi and H. E. Stanley, *Fractal Concepts in Surface Growth* (Cambridge University Press, 1995).
- [33] G. Blatter, M. V. Feigel'man, V. B. Geshkenbein, A. I. Larkin, and V. M. Vinokur, *Rev. Mod. Phys.* **66**, 1125 (1994).
- [34] T. Nattermann and S. Scheidl, *Advances in Physics* **49**, 607 (2000).
- [35] T. Giamarchi and S. Bhattacharya, in *High Magnetic Fields*, Lecture Notes in Physics, Berlin Springer Verlag, Vol. 595, edited by C. Berthier, L. P. Lévy, and G. Martinez (2002) pp. 314–360, [cond-mat/0111052](https://arxiv.org/abs/cond-mat/0111052).
- [36] P. Le Doussal, *International Journal of Modern Physics B* **24**, 3855 (2010).
- [37] C. H. Bennett, M. Büttiker, R. Landauer, and H. Thomas, *Journal of Statistical Physics* **24**, 419 (1981).
- [38] G. Tatara and H. Kohno, *Phys. Rev. Lett.* **92**, 086601 (2004).
- [39] V. Lecomte, S. E. Barnes, J.-P. Eckmann, and T. Giamarchi, *Phys. Rev. B* **80**, 054413 (2009).
- [40] S. E. Barnes, J.-P. Eckmann, T. Giamarchi, and V. Lecomte, *Nonlinearity* **25**, 1427 (2012).

[41] Even if the interface is started in an arbitrary  $h(r)$  configuration, it gradually flattens, and for  $t \rightarrow \infty$  the interface becomes flat if  $T = 0$ .

[42] A. M. Ettouhami and L. Radzihovsky, *Phys. Rev. B* **67**, 115412 (2003).

[43] We are implicitly assuming here that  $V(h) - f_0 h$  is quadratic around their minima. For a more general situation see the Appendix, Sec.A.

[44] J. S. Langer, *Phys. Rev. Lett.* **21**, 973 (1968).

[45] If the size of the optimal patch becomes of the order of the interface size a dimensional crossover is expected towards the zero dimensional or single particle result  $E_{max} \rightarrow \varepsilon^{3/2}$ .

[46] V. Ambegaokar and B. Halperin, *Physical Review Letters* **22**, 1364 (1969).

[47] A. Bishop and S. Trullinger, *Physical Review B* **17**, 2175 (1978).

[48] S. Habib and G. Lythe, *Phys. Rev. Lett.* **84**, 1070 (2000).

[49] As a matter of definition, the values of  $\Delta$  are calculated as the time interval between the time  $h$  crosses the value  $2\pi(n - 1/2)$  and the time in which it crosses the value  $2\pi(n + 1/2)$ .

[50] The strong decay of  $F_0(x)$  we observe by decreasing  $x$  and small temperatures makes it that in practice, it can be considered as a hard gap.

[51] The elastic force at the center of the kink is approximately zero, so it is only acted by the driving force  $f_c$ . In a small time interval  $\delta t$ , the interface at the kink position advances  $\delta h = f_c \delta t$  in the vertical direction and  $\delta x \approx \delta h \xi / 2\pi$  in the horizontal direction. Therefore  $c \approx f_c \xi / 2\pi$ .

[52] A. A. Middleton, *Phys. Rev. Lett.* **68**, 670 (1992).

[53] T. Nattermann, V. Pokrovsky, and V. M. Vinokur, *Phys. Rev. Lett.* **87**, 197005 (2001).

[54] M. Müller, D. A. Gorokhov, and G. Blatter, *Phys. Rev. B* **63**, 184305 (2001).

[55] L.-W. Chen and M. C. Marchetti, *Phys. Rev. B* **51**, 6296 (1995).

[56] L. Roters, A. Hucht, S. Lübeck, U. Nowak, and K. D. Usadel, *Phys. Rev. E* **60**, 5202 (1999).

[57] S. Bustingorry, A. B. Kolton, and T. Giamarchi, *EPL (Europhysics Letters)* **81**, 26005 (2007).

[58] S. Bustingorry, A. Kolton, A. Rosso, W. Krauth, and T. Giamarchi, *Physica B: Condensed Matter* **404**, 444 (2009).

[59] J. Gorchon, S. Bustingorry, J. Ferré, V. Jeudy, A. B. Kolton, and T. Giamarchi, *Phys. Rev. Lett.* **113**, 027205 (2014).

[60] R. Diaz Pardo, W. Savero Torres, A. B. Kolton, S. Bustingorry, and V. Jeudy, *Phys. Rev. B* **95**, 184434 (2017).

[61] N. Goldenfeld, *Journal of Physics A: Mathematical and General* **17**, 2807 (1984).

[62] X. Cao, S. Bouzat, A. B. Kolton, and A. Rosso, *Phys. Rev. E* **97**, 022118 (2018).